Chemical Engineering Journal 166 (2011) 496–503

Contents lists available at ScienceDirect

Chemical Engineering Journal

journal homepage: www.elsevier.com/locate/cej

Synthesis of iron-based adsorbents and their application in the adsorption of molybdenum ions in nitric acid solution

Gjergj Dodbiba[a,*], Toyohisa Fujita[a], Takahiro Kikuchi[b], Jayappa Manjanna[a], Seiji Matsuo[a], Hideyuki Takahashi[c], Kazuyuki Tohji[c]

[a] Department of Systems Innovation, Graduate School of Engineering, The University of Tokyo, 7-3-1 Hongo, Bunkyo-ku, Tokyo 113-8656, Japan
[b] Japan Atomic Energy Agency, Japan
[c] Department of Environmental Studies, Tohoku University, Japan

ARTICLE INFO

Article history:
Received 2 March 2010
Received in revised form 29 October 2010
Accepted 29 October 2010

Keywords:
Molybdenum
Nitric acid solution
Fe-based adsorbent
Adsorption
HLLW

ABSTRACT

A series of "easy-to-prepare" powders was synthesized and their application in the adsorption of Mo ions in 3 mol/L nitric acid solution was investigated. The powders were also calcinated at various temperatures, which effect was investigated as a function of the dissolved Fe concentration in the solution. In addition, the equilibrium sorption isotherm of Mo onto Fe-based adsorbent was analyzed by the Langmuir, Freundlich and Redlich–Peterson sorption models, whereas the adsorption kinetic was analyzed using the intraparticle diffusion model and the pseudo-second order kinetic model. The overall adsorption process was described well by the pseudo-second order kinetic model. It was found that the amount of Mo(VI) ion sorbed at equilibrium was 8.3126 mg/g, with 83% of Mo adsorption occurring the first 10 min and attaining equilibrium was at ca. 150 min. This behavior suggests that the sorption takes place rapidly on the external surface of the adsorbent where the binding may be through interaction with the functional groups located on the surface of the adsorbent.

1. Introduction

In order to minimize the long-term radiological risk and facilitate the management of high-level radioactive liquid waste (HLLW), several multi-cycle partition processes have been developed [1–6]. Generally speaking, a partition process is followed by vitrification of HLLW, which is an internationally recognized standard both to minimize the environmental impact resulting from the waste disposal and to reduce the volume of the waste [7–12].

Broadly speaking, alkali borosilicate glasses are the matrix of choice for the immobilization of the HLLW, since they permit vitrification of waste stream of different compositions. It has been reported that one problem with alkali borosilicates is that molybdenum (Mo), an element found in high concentration in HLLW, has a low solubility in this composition, and its presence in excess results in the phase separation of a complex yellow molten salt during vitrification [13]. The formation of so-called "yellow phase" material during the vitrification process is undesirable since it leads to the accelerated corrosion of the inconel crucible liners. Furthermore, the "yellow phase", which is reported to contain also other fission products (FP), is soluble in aqueous solution and thus providing a potential route for the leaching of radionuclides from the vitrified waste, should it come into contact with water [13]. In addition, Mo is one of the main fission products, since it represents 10 wt% of the total amount of FP in a spent fuel [14]. Thus, the removal of Mo will also significantly reduce the amount of HLLW to be disposed, as well as improve the vitrification of HLLW.

Since the incorporation of Mo is of particular concern in the vitrification of HLLW, Cruywagen and McKay [15] investigated the extraction by tri-n-butyl phosphate (TBP) of Mo(VI) from nitrate medium. Later, Smith et al. studied the recovery of various metals from simulated HLLW with hydrothermal crystallization, [16]. They showed that more than 35% of metals can be precipitated through hydrothermal crystallization. Fujii et al. [17], on the other hand, investigated the extraction of Mo ions using octyl(phenyl)-*N,N*-diisobutylcarbamoylmethylphosphine oxide, whereas Zhang et al. [14] synthesized a macroporous silica-based octyl(phenyl)-*N,N*-diisobutylcarbamoylmethylphosphine oxide impregnated polymeric composite to eliminate Mo from HLLW. Although the above mentioned composites can extract Mo from the HLLW (generally the extraction ratio varies between 90% and 95%), another material, such as a Fe-based adsorbent, could be a feasible and cost-efficient alternative.

In this work, a series of very "easy-to-prepare" iron-based adsorbents (hereafter also named as Fe-based adsorbent or FeBA for short) have therefore been synthesized in order to adsorb Mo(VI)

* Corresponding author at: Department of Systems Innovation, Graduate School of Engineering, The University of Tokyo, Eng. Bldg. 4, Room 424 7-3-1 Hongo, Bunkyo-ku, Tokyo 113-8656, Japan. Tel.: +81 3 5841 7080; fax: +81 3 5841 7080.
E-mail address: dodbiba@sys.t.u-tokyo.ac.jp (G. Dodbiba).

1385-8947/$ – see front matter © 2010 Elsevier B.V. All rights reserved.
doi:10.1016/j.cej.2010.10.079

ions from HNO_3 aqueous solution. The stability of the synthesized adsorbent in a HNO_3 aqueous solution containing Mo ions was primarily investigated by analyzing the dissolved Fe concentration as function of the calcination temperature of the adsorbent. In addition, using batch studies, the adsorption equilibrium, the adsorption kinetic, and the desorption of Mo from the loaded adsorbent were also investigated.

2. Materials and methods

2.1. Solution

A synthetic solution of Mo was prepared by dissolving ammonium molybdate $(NH_4)_6Mo_7O_{24}$, (Assay: 99%). The concentration of Mo in solution was similar to the concentration in a typical HLLW, where the Mo concentration varies from 890 to 1200 mg/L, [18–19]. The solution is made acidic with nitric acid, approximately 3 mol/L.

2.2. Synthesis of the iron-based adsorbents

Iron(III) chloride hexahydrate ($FeCl_3{\cdot}6H_2O$; Assay: 97%), and sodium hydroxide (NaOH; Assay 96%) were used without purification. Drops of sodium hydroxide solution (5 mol/L NaOH) were added in a 1 mol/L iron(III) chloride aqueous solution, until pH was adjusted at 13. The precipitate, which was removed from the supernatant by filtration, was then dried at 70 °C for over 72 h and ground using an agate mortar with pestle to obtain a fine powder that was used as an adsorbent. Prior to the adsorption experiment, the prepared powders were also calcinated at a temperature higher than 100 °C for 1 h, using a muffle furnace.

2.3. Effect of calcination temperature

In this set of experiments, the effect of the calcination temperature of the Fe-based adsorbent on the dissolved Fe concentration was investigated. Thus, the adsorbents were either dried at 70 °C for over 72 h or calcinated at 80, 210, 280, 350, 410, 500, 660, 700 or 800 °C for 1 h. Next, each adsorbent was added in a 3 mol/L HNO_3 aqueous solution. The initial Mo concentration (i.e. C_0) in each solution was 10.4 mmol/L (i.e. 996.3 mg/L), whereas the dosage of adsorbent was adjusted at 100 g/L. The samples were then mechanically stirred for 4 h. After filtering, the concentration of Fe ions in the supernatant was analyzed using an ICP-OES and the data were then reported in terms of the dissolved Fe concentration, d (i.e. mass of Fe/mass of adsorbent), which was calculated by using the following equation (Eq. (1)):

$$d = C_a \cdot \frac{V}{M} \quad (\mathrm{mg/g}), \tag{1}$$

where C_a is the aqueous concentration of Fe (in mg/L) after adsorption (note that the aqueous concentration of Fe before is 0 mg/L); V is the volume of sample (in L); M is the mass of the adsorbent (in g).

2.4. Quantitative and structure analysis of the synthesized adsorbents

Several Fe-based adsorbents, except where noted, samples were first calcinated at various temperatures (i.e. from 200 to 800 °C) for 1 h. Then the surface and the structure of each sample were analyzed using various equipments.

The chemical composition of the adsorbents was analyzed using the wavelength dispersive X-ray fluorescence (WDXRF) technique (WDXRF: Rigaku, WDXRF SuperMini). This analysis was repeated three times for each sample to provide an average reading. In addition, the structure of the synthesized adsorbents was analyzed by means of a X-ray diffractometer (XRD: Mac Science, MO3XHF) with Cu-Kα radiation (40 kV and 40 mA) at a scanning speed of 2°/min. The EXAFS spectra, on the other hand, were recorded with an extended X-ray adsorption fine structure spectrometer (EXAFS: Rigaku R-XAS Looper) at iron K-edge. The magnitude of Fourier transforms of the EXAFS spectra of the Fe-based adsorbent was then generated using standard procedures. The prepared powder sample (i.e. prior to calcination) was also used for thermogravimetric analysis (TG/DTA: Shimazu DTA-50). A few milligrams (16.2 mg) of iron-based adsorbent were used for the TG/DTA analysis. Moreover, alumina was used as the reference substance. The temperature was scanned between ambient and 1200 °C with a heating rate of 10 °C/min, while using air as the reactive gas.

2.5. Adsorption procedure and measurements

Prior to the experiment, Fe-based adsorbents were first calcinated at a given temperature for 1 h. In experiment, a known amount of the Fe-based adsorbent and 20 mL of 3 mol/L HNO_3 aqueous solution containing Mo ions, were mixed into a 50 mL clear plastic vial with lid and shaken mechanically for a period of time. Then, the sorbent was removed by filtration using a filter unit (pore size of 0.20 μm). Finally, the remaining concentration of Mo ions in the solution were analyzed using an inductively coupled plasma-optical emission spectrometer, ICP-OES (PerkinElmer, OPTIMA 5300DV). Next, the experimental results were reported in terms of the Mo sorbed concentration (i.e. mass of Mo/mass of adsorbent), which is also known as adsorption density. The sorbed amount of Mo, q was calculated using the following equation (Eq. (2)):

$$q = (C_0 - C_1) \cdot \frac{V}{M} \quad (\mathrm{mg/g}), \tag{2}$$

where C_0 and C_1 are aqueous concentration of adsorbate (in mg/L) before and after adsorption, respectively.

2.5.1. Evaluation of equilibria

The equilibrium relationship between the sorbed concentration q (in mg/g, Eq. (2)) and the adsorbate concentration C_1 in solution (in mg/L, Eq. (2)) is called adsorption isotherm. In order to collect the data to construct the isotherm, different amounts of the adsorbent were added in various samples of 3 mol/L HNO_3 solution containing 10.3 mmol/L Mo (i.e. 986.8 mg/L), and mechanically shaken for 3 h. After filtering, the remaining concentration of Mo in solution was measured by ICP-OES. By knowing the initial and the remaining concentrations of Mo ions, the sorbed Mo concentration q was calculated, (Eq. (2)). The data were then analyzed using the Langmuir, Freundlich and Redlich–Peterson models.

2.5.2. Adsorption kinetics

In this series of test, the initial concentration of Mo ion in a 3 mol/L HNO_3 solution was adjusted at 9.5 mmol/L (i.e. 911.1 mg/L), whereas the adsorbent dosage was 100 g/L. The contact time was varied from 1 to 300 min. The remaining concentration of Mo ion was then measured by ICP-OES. The data were then analyzed using the intraparticle diffusion and pseudo-second-order kinetic models.

2.6. Desorption procedure

In experiment, 2 g of the Fe-based adsorbent, which was calcinated at a given temperature for 1 h, and 20 mL of 3 mol/L HNO_3 aqueous solution containing 918 mg/L Mo(VI), were first mixed and shaken mechanically for 4 h. After adsorption of Mo(VI), the 0.2 g of loaded adsorbent, which was removed by filtration using a filter unit (pore size of 0.20 μm), was immersed in a flask containing

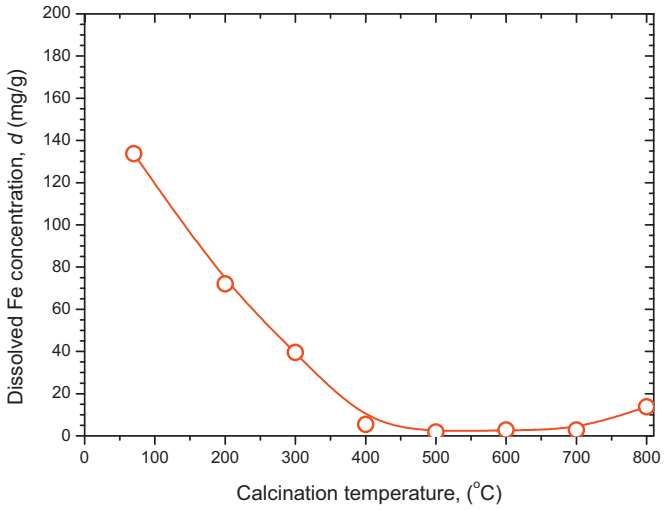

Fig. 1. Dissolved Fe concentration as a function the calcination temperature of the Fe-based adsorbent; (*experimental conditions*: solution: 3 mol/L HNO_3; initial concentration of Mo ions: 10.4 mmol/L (i.e. 996.3 mg/L); dosage of Fe-based adsorbent: 100 g/L; contact time: 4 h.).

20 mL NaOH solution of known molarity. The flask was then placed in a thermostated water bath at 85 °C and once again was shaken mechanically for 4 h. After desorption of Mo(VI), the adsorbent was removed by filtration and was dissolved in a known volume of HCl solution. Finally, the concentration of Mo(VI) in the HCl solution was analyzed using an ICP-OES. The experimental results were then reported in terms of the desorption yield e that was calculated by the following equations, (Eq. (3)):

$$e = \frac{(q - q_R)}{q} \cdot 100 \quad (\%), \tag{3}$$

where q_R is the remaining amount of adsorbate in the adsorbent, (mass adsorbate/mass adsorbent, mg/g).

The desorption yield of Mo from the loaded adsorbent, was investigated as a function of the molarity of the NaOH solution, keeping the dosage of adsorbent in solution constant at 10 g/L.

3. Results and discussion

3.1. Effect of calcination temperature of the Fe-based adsorbent

In order to investigate the effect of temperature, when preparing the Fe-based adsorbent, various adsorbents were first calcination at different temperatures, before being used in experiment. The experimental results shown in Fig. 1 indicate the effect of calcination temperature of the adsorbent on the dissolved Fe concentration. Referring to these experimental results, the calcination temperature had a great influence on the dissolved Fe concentration. Fig. 1 shows that when the adsorbent was calcinated at 500 °C or higher, the dissolve Fe concentration was relatively low. Note that when the adsorbent was calcinated at 500 °C, the dissolve Fe concentration was the lowest, i.e. 1.9 mg/g. In other words, the experimental results suggested that the calcination of the adsorbent at 500 °C, prior to the adsorption experiments, is effective in substantially reducing the dissolved concentration of Fe in 3 mol/L nitric acid solution containing Mo ions. Considering the results shown in Fig. 1, the Fe-based adsorbent was calcinated at 500 °C, before being used in all subsequent experiments.

Table 1
Elemental composition of Fe-based adsorbent (Unit: mass%).

Type of adsorbent	Elements		
	Na	Cl	Fe
Before calcination	23.1	24.9	52
After calcination at 500 °C	7.28	0.02	92.7

3.2. Characterization of the adsorbent

Following is a series of quantitative and qualitative measurements carried out to analyze the Fe-based adsorbent.

3.2.1. WDXRF and XRD analysis

The elemental composition of Fe-based adsorbent, analyzed by WDXRF technique, is given in Table 1. The results indicated the presence of Fe as major constituent and with subordinate Na and Cl, which contaminated the surface of the adsorbent during its synthesis.

The aim of the X-ray diffraction analysis (XRD), on the other hand, was to observe the structure evolution of the Fe-based adsorbent as a function of the calcination temperature. The diffraction patterns for the Fe-based adsorbents, calcinated at different temperatures are shown in Fig. 2.

X-ray diffraction analysis showed that when the adsorbent is calcinated at a temperature lower than 300 °C, the number of count for these phases was low, indicating that their structure is predominately amorphous. For instance, Fig. 3 shows that when adsorbent is calcinated at 70 °C, 200 or 300 °C no crystalline structure was observed. Nevertheless, when the adsorbent is calcinated at 400 °C or higher, hematite (Fe_2O_3) was the only crystalline phase being observed. It was also observed that the intensity of the hematite peaks increased with raising calcination temperature.

3.2.2. EXAFS analysis

The periodic oscillation, which appears in an absorption spectrum on the high-energy side of the X-ray adsorption edge (typically 50 eV–1000 eV), is called extended X-ray absorption fine structure (EXAFS), [20]. EXAFS is due to scattering of the ejected photoelectron by atoms of surrounding the adsorbing atom and therefore provides information on the local structure around the selected X-ray adsorption atom, [21].

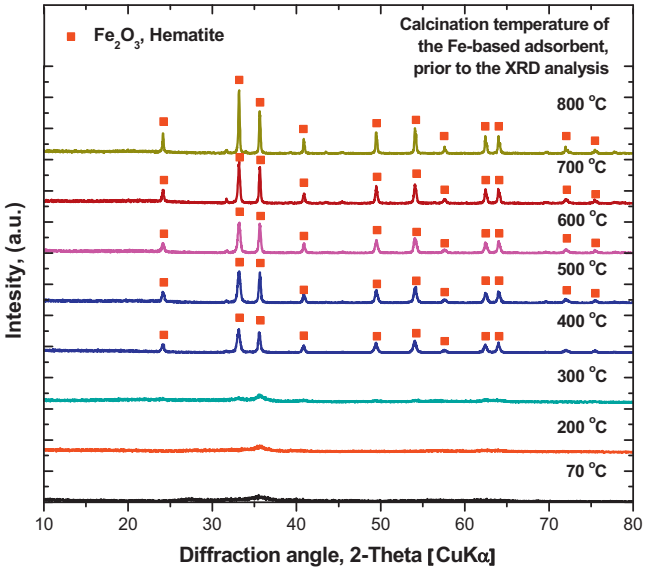

Fig. 2. XRD pattern of the Fe-based adsorbent, after calcination at different temperatures for 1 h. *Note*: All the XRD analyses were performed at room temperature.

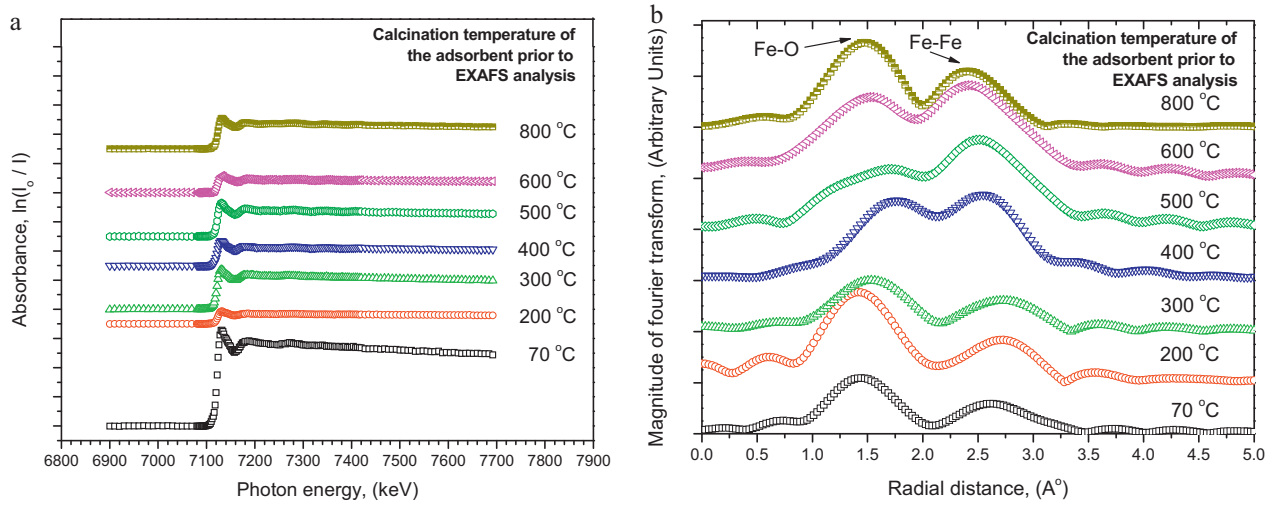

Fig. 3. Spectra (a) and magnitude of Fourier transforms of the Fe K-edge EXAFS spectra (b) of the Fe-based adsorbent, calcinated at different temperatures.

In recent years EXAFS technique is gaining popularity since it has been recognized as a valuable tool for the determination of the structure of the mater [22]. Besides, EXAFS is best suited to trace a procedure of synthesis. The point-scattering theory of EXAFS is widely used to obtain the interatomic distances around a particular atomic species. The interatomic distances, on the other hand, is related to the threshold energy E_o associated with the ejection of the photoelectron, [23–24].

Fig. 3(a) shows the EXAFS spectra of the adsorbents, calcinated at different temperatures, whereas Fig. 3(b) shows the magnitude of Fourier transforms of the Fe K-edge EXAFS spectra. The Fourier transform of all EXAFS spectra around Fe atom exhibited two distinct peaks at 1.4–1.7 Å and 2.4–2.7 Å, (Fig. 3(b). The first intense peak is due to backscattering from the neighboring oxygen atom (i.e. the Fe–O bondlength), whereas the second one, weaker peak at a longer distance, is due to backscattering from the neighboring iron atom (i.e. the Fe–Fe bondlength).

Fig. 4 shows the changes in the predicted bondlengths, extrapolated from the results of the EXAFS analysis (Fig. 3b), as a function of calcination temperature. The most immediate conclusion that can be drawn from these results is that the calcination temperature of the adsorbent had a great effect on both bondlengths. Changes in the Fe–O distance provide independent evidence of the oxidation of Fe. Note that at about 500 °C, the Fe–O bondlength is the longest, whereas the Fe–Fe bondlength is relatively short, (Fig. 4). Fig. 4 also shows that when the adsorbent was calcinated at 500 °C or higher, both interatomic distances (i.e. Fe–Fe and Fe–O) decreased with increasing temperature. Thus, the short interatomic distances gave rise to a relative large threshold energy E_o [25], which suggest the stability against reduction [26]. In other words, these changes in bondlengths (especially Fe–Fe bondlength) may be ascribed to stability of the adsorbent and therefore to a very low concentration of Fe, dissolved in HNO_3 aqueous solution, (Fig. 1).

3.2.3. TG/DTA analysis

Fig. 5 shows the recorded thermograms. Two main peaks are observed in the DTA thermogram in which the heat is absorbed or evolved from the adsorbent. The first peak indicated that sample begins to crystallize as microcrystals at 120 °C, giving off heat in the process. The second main peak at ca. 450 °C is the result of another change in structure. The authors think that the second peak represents the Fe–Fe and Fe–O bondlengths changes of adsorbent, (Fig. 4).

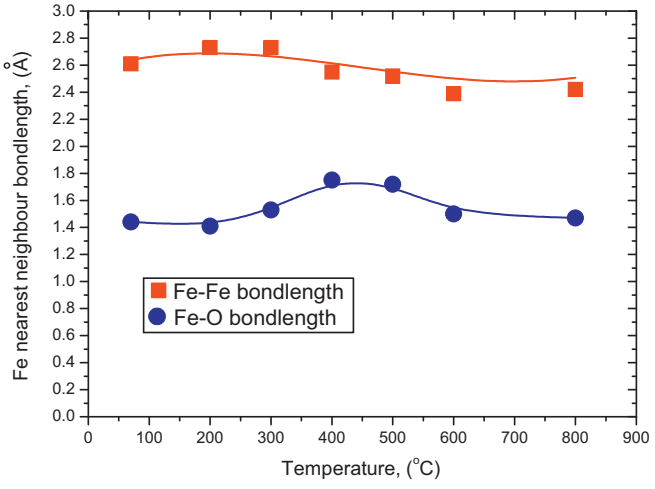

Fig. 4. The predicted lengths of Fe–Fe and Fe–O bonds as a function of the calcination temperature of the Fe-based adsorbent.

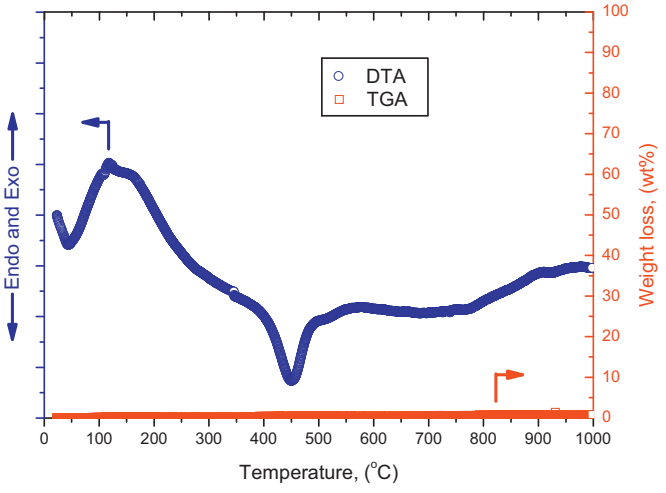

Fig. 5. Thermogram for Fe-based absorbent. (*Note*: no calcination of adsorbent was carried out prior to the analysis; heating rate: 10 °C/min; reactive gas: Air.)

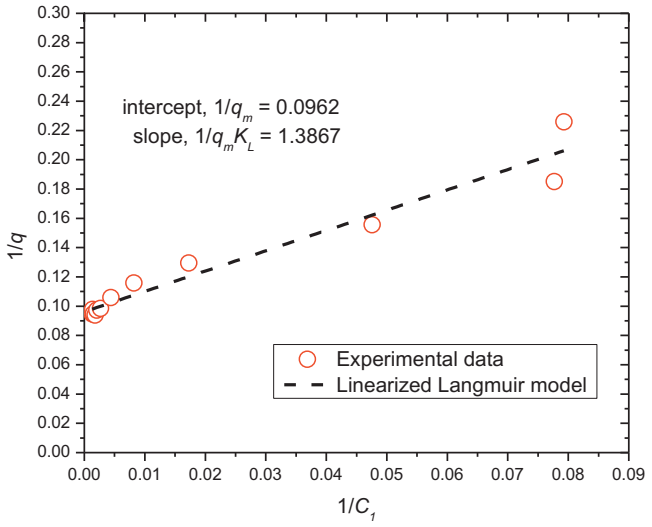

Fig. 6. Linear graph of the Langmuir isotherm (*Experimental conditions:* solution: 3 mol/L HNO_3; initial concentration of Mo ions: 10.3 mmol/L (i.e. 986.8 mg/L); contact time: 3 h.).

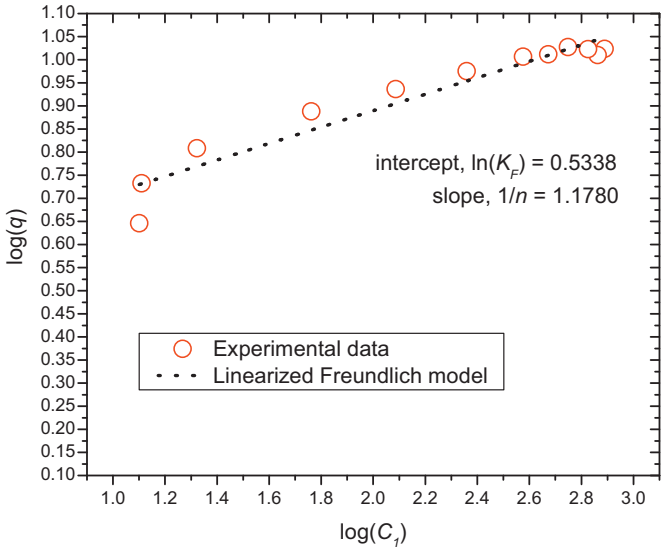

Fig. 7. Linear graph of the Freundlich isotherm (|*Experimental conditions:* solution: 3 mol/L HNO_3; initial concentration of Mo ions: 10.3 mmol/L (i.e. 986.8 mg/L); contact time: 3 h.).

3.3. Adsorption isotherm of Mo ions onto the Fe-based adsorbent

Generally speaking, the analysis of the isotherm data is important to develop an equation which could represent the results and be used for designing purposes. In order to model the sorption isotherm of Mo from 3 mol/L HNO_3 aqueous solution, the Langmuir, Freundlich and Redlich–Peterson models were used.

The Langmuir's model, which was originally formulated for gas adsorption on homogeneous surfaces, [27], was extended to adsorption of metal ions from solution, [28]. The model is characterized by linear adsorption at low surface coverage, which becomes non-linear as adsorption sites approach saturation. In other words, the Langmuir model (Eq. (4)) assumes that the surface of the adsorbent is homogeneous and solute uptake occurs by monolayer adsorption, since the adsorption energy is uniform for each site:

$$q_e = q_m \frac{K_L C_1}{1 + K_L C_1} \tag{4}$$

where q_m is the maximum capacity of the adsorbent for adsorbate, (mass adsorbate/mass adsorbent, mg/g); and K_L (L/mg) is a measure of affinity of adsorbate for adsorbent.

The linearized form of the Langmuir isotherm, is given by Eq. (5), [27,29]. The maximum capacity q_m and K_L are then determined directly from the intercept and the slope of the straight line of the linearized form of the isotherm, (Eq. (5)).

$$\frac{1}{q} = \frac{1}{q_m K_L}\left(\frac{1}{C_1}\right) + \frac{1}{q_m} \tag{5}$$

Fig. 6 shows $1/q$ versus $1/C_1$ for adsorption of Mo onto the Fe-based adsorbent, calcinated at 500 °C. The data have then been extrapolated using the least-squared linear regression in order to calculate the maximum capacity of the adsorbent (q_m). The experimental data were well fitted to the linear form of Langmuir equation (Eq. (5)) with a correlation coefficient $R^2 = 0.9815$, indicating the applicability of the model. It was found that the Langmuir isotherm (Eq. (5)) gives $q_m = 10.3950$ mg/g and $K_L = 0.0694$ L/mg, (Fig. 6).

The Freundlich isotherm [30] is the earliest known relationship, which assumes that the surface sites of the adsorbent have different binding energies. The Freundlich expression is an empirical equation describing adsorption onto heterogeneous surfaces and is expressed as, (Eq. (6)):

$$q = K_F C^{1/n} \tag{6}$$

where K_F (mg/g), which indicates the adsorption capacity, and n are both empirical constants. The value of n indicates a favorable adsorption for $1 < n < 10$.

The linearized form of isotherm is given as, (Eq. (7)):

$$\ln q = \ln K_F + \frac{1}{n} \ln C \tag{7}$$

Both constants K_F and n are then determined directly from the intercept and the slope of the straight line of the linearized form of the isotherm, (Eq. (7)).

Fig. 7 shows $\ln(q)$ versus $\ln(C)$ for adsorption of Mo onto the Fe based adsorbent. The data have then been extrapolated using the least-squared linear regression in order to calculate K_F and n. It was found that the Freundlich isotherm gives $K_F = 1.7054$ mg/g and $n = 5.6170$, (Fig. 7).

The Redlich–Peterson isotherm model [31], on the other hand, includes features of both Langmuir and Freundlich isotherm. It is expressed as:

$$q = \frac{K_{R-P} C}{(1 + a C^g)} \tag{8}$$

where K_{R-P} (L/g) and a are the isotherm constants, whereas g is an exponent, which varies from 0 to 1 (i.e. $0 < n < 1$). All three constants were evaluated using the generalized reduced gradient (GRG2) non-linear optimization code. The results of calculation indicated that the Redlich–Peterson isotherm constants are: $K_{R-P} = 696.9696$ (L/g), $a = 187.2101$ and $g = 0.8373$.

The experimental data were then fitted to the Langmuir model (Eq. (4)), the Freundlich model (Eq. (6)) and the Redlich–Peterson model (Eq. (8)) and plotted in Fig. 8 together with the experimental results. Comparing all three models, (Table 2 and Fig. 8), the authors suggest that the Langmuir model is more suitable than the other two models, since is gives the highest value for R^2.

3.4. Adsorption kinetics of Mo ions onto the Fe-based adsorbent

Many adsorption kinetic models have been reported, [32]. The intraparticle diffusion model [33] and the pseudo-second-order kinetic [34] are among the most widely applied.

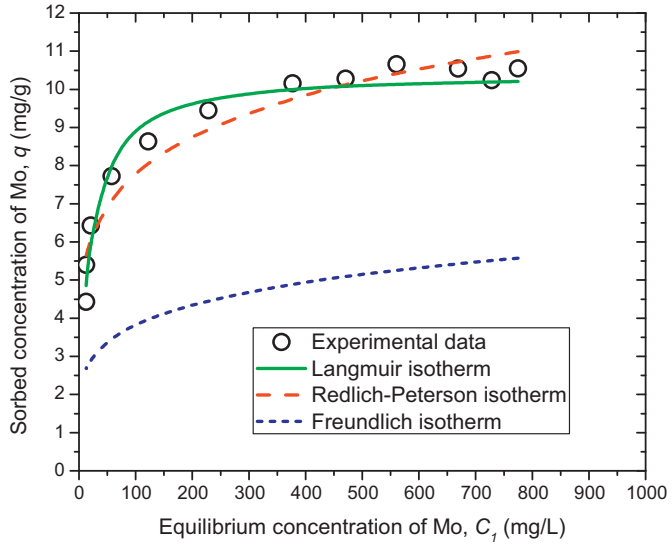

Fig. 8. Adsorption of Mo onto the Fe-based adsorbent, calcinated at 500 °C (*Experimental conditions:* solution: 3 mol/L HNO_3; initial concentration of Mo ions: 10.3 mmol/L (i.e. 986.8 mg/L); Contact time: 3 h.).

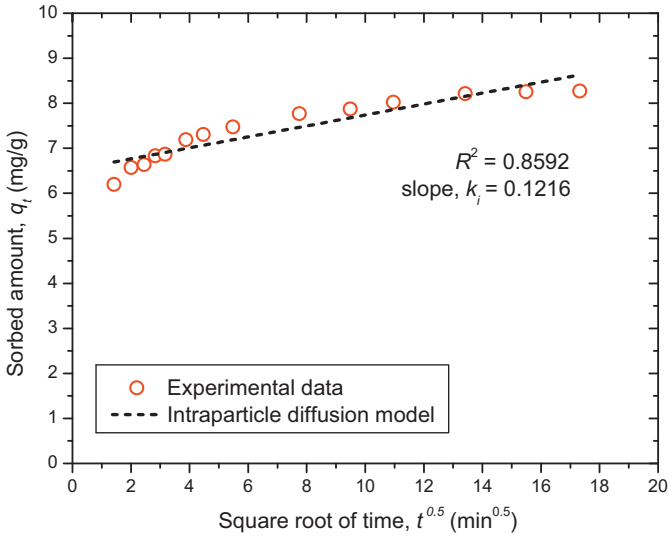

Fig. 9. Intraparticle diffusion kinetics of Mo ions onto Fe-based adsorbent, calcinated at 500 °C (*Experimental conditions:* solution: 3 mol/L HNO_3; initial concentration of Mo ions: 9.5 mmol/L (i.e. 911.1 mg/L); dosage of the Fe-based adsorbent, calcinated at 500 °C: 100 g/L.).

Broadly speaking, the diffusion models are particularly important where ion exchange or ionic bonding is not as prevalent as in chemisorption processes. According to the theory proposed by Weber and Morris [35], a functional relationship common to most treatments of intraparticle diffusion is that uptake q_t varies almost with the square root of time $t^{0.5}$. The linear form of the intraparticle diffusion equation is give as:

$$q_t = k_i t^{0.5} \tag{9}$$

where k_i is the intraparticle diffusion rate constant, (mg/g $min^{0.5}$). If the intraparticle diffusion is the only mechanism taking place, a plot of adsorption capacity q_t at time t versus $t^{0.5}$ would yield a straight line. The k_i value is then calculated from the slope of the straight line. The plot might have more than one "linear segments" or "portions". The initial steep "segment" is attributed to the diffusion of adsorbate through the boundary layer diffusion of solute molecules or the external surface of the adsorbent. The second "segment" describes the gradual adsorption stage, whereas the third "segment" of the plot is attributed to the final equilibrium stage where intraparticle diffusion starts to slow down due to the extremely low concentration of adsorbate in the solution. Fig. 9 shows the intraparticle diffusion plot, which do not pass through the origin, indicating that the intraparticle diffusion is not the only operative mechanism. As it can be seen in Fig. 9, the external surface adsorption (i.e. the first portion or segment of the plot) is absent; apparently it is completed before the first 4 min. It was found that the correlation coefficient R^2 was greater than 0.85 (Fig. 9), but not as great as might have been expected.

Table 2
Comparing Langmuir, Freundlich and Redlich–Peterson sorption isotherm models for adsorption of Mo ions onto the Fe based adsorbent, calcinated at 500 °C.

Model	Parameters of the model	Correlation coefficient, R^2
Langmuir isotherm		0.9815
K_L (L/mg)	0.0694	
q_m (mg/g)	10.3950	
Freundlich isotherm		0.9685
K_F (mg/g)	1.7054	
n	5.6170	
Redlich–Peterson isotherm		0.9701
K_{R-P} (L/g)	696.9696	
a	187.2101	
g	0.8373	

The pseudo-second order equation, on the other hand, assumes that adsorption behavior is controlled by a second-order reaction. The equation is expressed as follows:

$$\frac{dq_t}{dt} = k(q_e - q_t)^2 \tag{10}$$

where q_e is the amount of metal ion sorbed at equilibrium (mg/g), q_t is the amount of metal ion sorbed at time t (mg/g), and k is the rate constant of the pseudo-second order kinetic model of adsorption, (g/mg min). Integrating Eq. (10) for the boundary conditions ($t = 0$) to ($t = t$) and ($q_t = 0$) to ($q_t = q_t$), gives:

$$\frac{1}{(q_e - q_t)} = \frac{1}{q_e} + kt \tag{11}$$

The linearized form of Eq. (11), which is the integrated rate law for a pseudo-second order reaction, is given by Eq. (12):

$$\frac{t}{q_t} = \frac{1}{kq_e^2} + \frac{1}{q_e}t \tag{12}$$

If pseudo-second order kinetic is applicable, the plot of t/q_t versus t can yield a straight line, from which q_e and k can then be determined from the slope and the intercept of the line. In addition, the Eq. (11) can also be arranged to obtain:

$$q_t = \frac{q_e^2 kt}{(1 + q_e kt)} \tag{13}$$

Fig. 10 shows a plot of Eq. (12) for the sorption of Mo using Fe-based adsorbent, calcinated at 500 °C. The results indicate a very significant linear relationship between t/q_t and t, with very high correlation coefficient, R^2. It was found that the pseudo-second-order reaction (Eq. (12)) gives q_e = 8.3126 mg/g and k = 0.0495 g/mg min, (Fig. 10). The perfect fit of the experimental data indicates the applicability of the pseudo-second order kinetic model for the adsorption of the Mo ions onto the prepared adsorbent. The pseudo-second order kinetics indicates that the adsorption of Mo onto adsorbent is involved in a rate determining step, which might be a chemical sorption or chemisorption, [36].

Comparing the correlation coefficients for both models, (Table 3), the authors suggest that the pseudo-second order equation is more suitable than the intraparticle model, indicating that

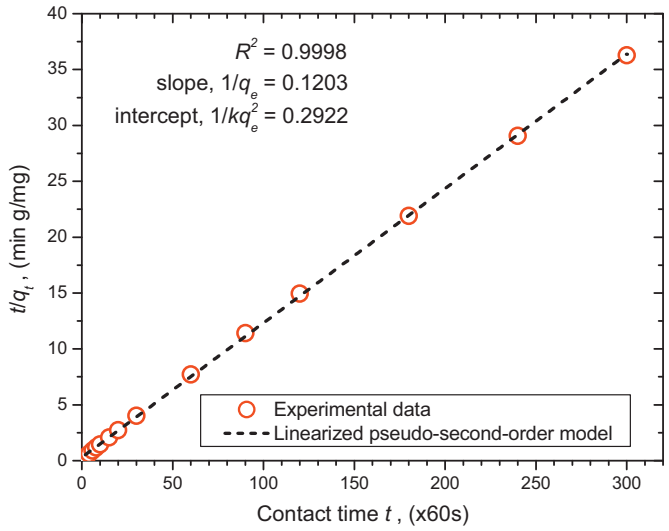

Fig. 10. Pseudo-second order sorption kinetics of Mo ions onto Fe-based adsorbent, calcinated at 500 °C (*Experimental conditions:* solution: 3 mol/L HNO_3; Initial concentration of Mo ions: 9.5 mmol/L (i.e. 911.1 mg/L); dosage of the Fe-based adsorbent, calcinated at 500 °C: 100 g/L.).

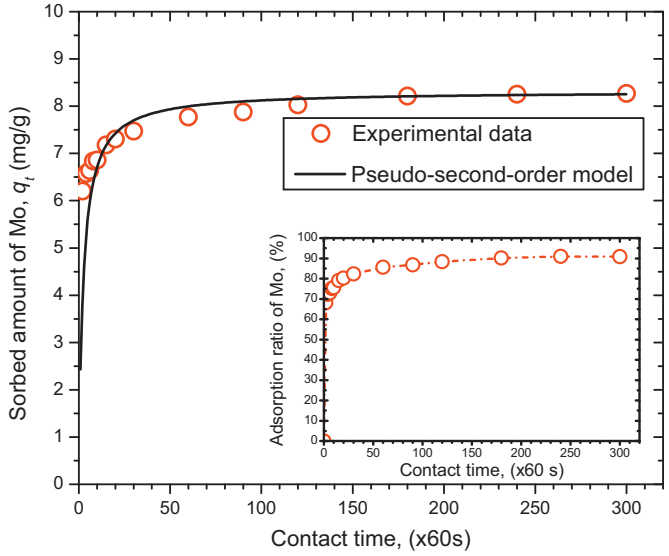

Fig. 11. A plot of the sorbed amount of Mo ions onto Fe-based adsorbent as a function of contact time (*Experimental conditions:* solution: 3 mol/L HNO_3; initial concentration of Mo ions: 9.5 mmol/L (i.e. 911.1 mg/L); dosage of the Fe-based adsorbent, calcinated at 500 °C: 100 g/L.).

chemisorption is the rate controlling step and therefore the sorption of Mo ions onto Fe-based adsorbent may be chemically rate controlling.

The experimental data were then fitted to the integrated pseudo-second-order equation (Eq. (13)) and shown in Fig. 11. The inset in Fig. 11 shows that sorbed amount of Mo ions onto adsorbent was rapid, with 83% of Mo adsorption occurring the first 10 min and attaining equilibrium was at ca. 150 min. This behavior suggests

Table 3
Comparing intraparticle diffusion model with pseudo-second order kinetic model for adsorption of Mo ions onto the Fe-based adsorbent, calcinated at 500 °C.

Model	Initial concentration, C_0 (mg/L)	Correlation coefficient, R^2
Intraparticle diffusion model	911.1	0.8592
Pseudo-second order sorption kinetic	911.1	0.9998

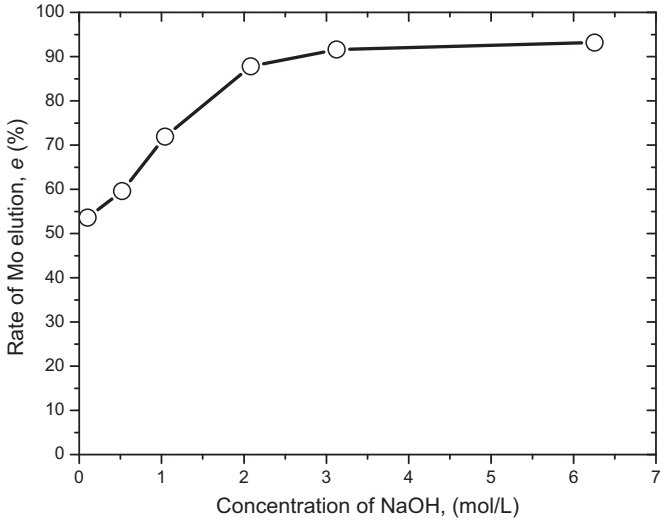

Fig. 12. Yield of Mo(VI) desorption as a function of the concentration of NaOH (*Experimental conditions:* dosage of loaded Fe-based adsorbent: 10 g/L; temperature: 85 °C; contact time: 4 h.).

that the sorption takes place rapidly on the external surface of the adsorbent where the binding may be through interaction with the functional groups located on the surface of the adsorbent.

3.5. A possible adsorption mechanism

The ionic state of molybdenum in aqueous solution has already been studied extensively. It has been reported that when the concentration of HNO_3 is higher than 1 mol/L, the divalent mononuclear cation of MoO_2^{2+} is the predominant species, [17,37–38]. In addition, considering the ≡FeBA groups on the surface of the adsorbent, be "half in solution and half out", they can become protonated and forming a species ≡(FeBA)H^+. Thus, the adsorption of Mo(VI) by FeBA adsorbent can be described by the following equation (Eq. (14)):

$$\equiv \mathrm{FeBA} + \mathrm{MoO_2^{2+}} + 3\mathrm{NO_3^-} + \mathrm{H^+} \leftrightarrow \equiv (\mathrm{FeBA})\mathrm{H^+} \cdot \mathrm{MoO_2(NO_3)_3^-} \quad (14)$$

It should be noted that the reaction between Mo(VI) ion and the FeBA needs further investigation, since the type of Mo(VI) species as well as the transformation between Mo(VI) species in HNO_3 aqueous solution are not completely understood yet. Nevertheless, the adsorption of Mo(VI) can be attributed to the affinity of the oxygen atom in FeBA for MoO_2^{2+}, which results in formation of a stable complex species. The authors suggest that calcination of adsorbent leads to changes in structure and surface of adsorbent, which result in an enhanced affinity of FeBA's surface for Mo(VI) ions. The reason is that when the adsorbent was calcinated at 500 °C, the Fe–O bondlength is relatively long (Fig. 4), indicating a reduced threshold energy E_o. This, in other words, suggests an enhanced affinity of adsorbent for MoO_2^{2+} ions. The affinity of the oxygen atom in FeBA for MoO_2^{2+} is therefore related to length of the Fe–O bond in FeBA adsorbent.

3.6. Desorption of Mo ions from the loaded Fe-based adsorbent: effect of NaOH concentration

In order to achieve practical adsorption, the adsorbate has to be desorbed and the spent adsorbent reused. Thus, Mo(VI) was first adsorbed using the Fe-based adsorbent, calcinated at 500 °C for 1 h, before being used in the desorption experiment. The experimental results showed that the yield of Mo(VI) desorption sharply increased with increasing molarity of NaOH solution, (Fig. 12).

Fig. 12 shows that the desorption yield reached at about 92% when the concentration of NaOH was adjusted at 3 mol/L. The basicity of the solution and therefore the concentration of NaOH seems to be an important factor for desorption of Mo ions, since the binding of metal ions by surface functional groups is strongly pOH dependent [39]. Nevertheless, more work is needed to better understand the desorption mechanism.

4. Conclusions

A series of "very easy-to-prepare" Fe-based adsorbents were synthesized in order to adsorb Mo(VI) from nitric acid (HNO_3) aqueous solution. The adsorbents were collected by filtration after a precipitate was formed by adding sodium hydroxide in a 1 mol/L iron(III) chloride aqueous solutions. In addition, the adsorbents were also calcinated at various temperatures, which effect was investigated as a function of the dissolved Fe concentration in the solution.

The equilibrium sorption isotherm of Mo onto Fe-based adsorbent was better described by the Langmuir isotherm equation with correlation coefficients of 0.9815. Moreover, the adsorption kinetic was analyzed using both the intraparticle diffusion model and pseudo-second order kinetic model. The overall adsorption process was described well by the pseudo-second order kinetic model (R^2 = 0.9998). It was found that the amount of Mo(VI) ion sorbed at equilibrium was 8.3126 mg/g, with 83% of Mo adsorption occurring the first 10 min and attaining equilibrium was at ca. 150 min.

Another important finding of this work was when the adsorbent was calcinated at 500 °C or higher, both interatomic distances (i.e. Fe–Fe and Fe–O) decreased with increasing temperature. These changes in bondlengths (especially Fe–Fe bondlength) may be ascribed to the stability of the adsorbent and therefore to a very low concentration of Fe, dissolved in HNO_3 aqueous solution. In addition, the Fe–O bondlength was relatively long, when the adsorbent was calcinated at 500 °C, which suggests that the affinity of the FeBA for MoO_2^{2+} is therefore related to length of the Fe–O bond in FeBA.

Acknowledgements

The present study includes the result of "Development of separation technology of transuranium elements and fission products using new extractants and adsorbents" entrusted to Japan Atomic Energy Agency by the Ministry of Education, Culture, Sports, Science and Technology of Japan (MEXT). This research was also supported in part through the Global COE Program, "Global Center of Excellence for Mechanical Systems Innovation," by MEXT. In addition, the authors gratefully acknowledge the technical support provided by Mr. Kazuhiro Fukawa of the University of Tokyo in caring out the XRD analysis.

References

[1] L. Koch, Minor actinide transmutation – a waste management option, Journal of the Less-Common Metals 122 (1986) 371–382.
[2] W.W. Schulz, E.P. Horwitz, TRUEX process and the management of liquid TRU waste, Separation Science and Technology 23 (12-13) (1988) 1191–1210.
[3] H. Eccles, Nuclear fuel cycle technologies – sustainable in the twenty first century? Extraction and Ion Exchange 18/4 (2000) 633–654.
[4] J.N. Mathur, M.S. Murali, K.L. Nash, Actinide partitioning – a review, Solvent Extraction and Ion Exchange 19/3 (2001) 357–390.
[5] A. Zhang, Y. Wei, M. Kumagai, Y. Koma, A new partitioning process for high-level liquid waste by extraction chromatography using silica-substrate chelating agent impregnated adsorbent, Journal of Alloys and Compounds 390 (2005) 275–281.
[6] T. Sasa, K. Nishihara, T. Sugawara, Y. Okamoto, H. Oigawa, Actinide reformer concept, Progress in Nuclear Energy 50 (2–6) (2008) 353–358.
[7] E. Ewest, H. Wiese, High level liquid waste vitrification with the PAMELA plant in Belgium, in: Proc. an Int. Conf.: Nuclear Power Performance and Safety, 5, 1988, pp. 269–280.
[8] O.L. Kruger, R.A. Watrous, G.F. Piepel, Progress in the development of glass compositions for vitrification of Hanford high-level transuranic wastes, Transactions of the American Nuclear Society 61 (1990) 52–53.
[9] I.A. Sobolev, A.S. Barinov, F.A. Lifanov, A.P. Kobelev, V.I. Kornev, A.E. Savkin, The development of technological process and pilot plant for vitrification of liquid intermediate level wastes, Transactions of the American Nuclear Society 67/1 (1993) 366–367.
[10] T. Fujii, H. Yamana, M. Watanabe, H. Moriyama, Extraction study for TREX process using short-lived radionuclides produced by neutron irradiation of uranium, Solvent Extraction and Ion Exchange 20/2 (2002) 151–175.
[11] R. Do Quang, V. Petitjean, F. Hollebecque, O. Pinet, T. Flament, A. Prod'homme, Vitrification of HLW produced by uranium/molybdenum fuel reprocessing in COGEMA's cold crucible melter, in: Proc. of the 9th Int. Conf. on Environmental Remediation and Radioactive Waste Management, 3, 2003, pp. 1585–1591.
[12] V. Brown, Nuclear waste: with plutonium, even ceramics may slump, Science 315 (2007) 174.
[13] R.J Short, R.J. Hand, N.C. Hyatt, G. Möbus, Environment and oxidation state of molybdenum in simulated high level waste glass compositions, Journal of Nuclear Materials 340 (2005) 179–186.
[14] A. Zhang, E. Kuraoka, M. Kumagai, Removal of Pd(II), Zr(IV), Sr(II), Fe(III), and Mo from simulated high level liquid waste by extraction chromatography utilizing the macroporous silica-based polymeric materials, Separation and Purification Technology 50 (2006) 35–44.
[15] J.J Cruywagen, H.A.C. McKay, The extraction of molybdenum(VI) by tri-*n*-butyl phosphate, Journal of Inorganic Nuclear Chemistry 32 (1970) 255–265.
[16] R.L. Smith, P. Atmaji, Y. Hakuta, M. Kawaguchi, T. Adschiri, K. Arai, Recovery of metals from simulated high-level liquid waste with hydrothermal crystallization, The Journal of Supercritical Fluids 11 (1997) 103–114.
[17] T. Fujii, H. Yamana, M. Watanabe, H. Moriyama, Extraction of molybdenum from nitric acid by octyl(phenyl)-N,N-diisobutylcarbamoylmethyl-phosphine oxide, Solvent Extraction and Ion Exchange 19/1 (2001) 127–141.
[18] H. Kleykamp, The chemical state of the fission' products in oxide fuels, Journal of Nuclear Materials 131 (1985) 221–246.
[19] P.R. Gray, Separation of cesium from fission product waste solutions, Journal of Inorganic and Nuclear Chemistry 12 (1960) 304–314.
[20] L.V. Azároff, Theory of extended fine structure of X-ray absorption edges, Reviews of Modern Physics 35 (1963) 1012–1021.
[21] D.E. Sayers, E.A. Stern, F.W. Lytle, New technique for investigating noncrystalline structures: Fourier analysis of the extended X-ray-absorption fine structure, Physical Review Letters 27 (1971) 1204–1207.
[22] K. Tohji, Y. Udagawa, S. Tanabe, A. Ueno, Catalyst preparation procedure probed by EXAFS spectroscopy, Journal of the American Chemical Society 106 (1984) 612–617.
[23] K. Asakura, Analysis of EXAFS, in X-ray adsorption fine structure for catalysts and surfaces, in: Y. Iwasawa (Ed.), X-ray Absorption Fine Structure for Catalysts and Surfaces, World Scientific, 1996, pp. 33–58.
[24] W.R. Flavell, in: J.C. Vickerman (Ed.), Absorption/Scattering Techniques in Surface Analysis – The Principal Techniques, John Wills & Sons, 1997, pp. 346–391.
[25] H. Maeda, Accurate bond length determination by EXAFS method, Journal of the Physical Society of Japan 56/8 (1987) 2777–2787.
[26] R.W. Joyner, M. Stockenhuber, Unusual structure and stability of iron-oxygen nano-clusters in Fe-ZSM-5 catalysts, Catalysis Letters 45 (1997) 15–19.
[27] I. Langmuir, The constitution and fundamental properties of solids and liquids, Journal of the American Chemical Society 38 (1916) 2221–2295.
[28] A.W. Adamson, Pysical Chemistry of Surfaces, fourth ed., John Willey & Sons, New York, 1984.
[29] M.M. Benjamin, Water Chemistry, McGraw-Hill, New York, 2002.
[30] H.M.F. Freundlich, Adsorption in solids, Zeitschrift fuer Physikalische Chemie Stoechiometrie und Verwandtschaftslehre 57 (1906) 385–470.
[31] O. Redlich, D.L. Peterson, A useful adsorption isotherm, Journal of Physical Chemistry 63 (1959) 1024.
[32] S. Yiancoumi, C. Tien, Kinetics of Metal Ion Adsorption from Aqueous Solutions: Models, Algorithms, and Applications, Kluwer Academic Publisher, 1995.
[33] J. Crank, The Mathematics of Diffusion, Clarendon Press, Oxford, 1979.
[34] Y.S. Ho, G. McKay, Pseudo-second order model for sorbtion processess, Process Biochemistry 34 (1999) 451–465.
[35] J.R. Weber, J.C. Morris, Kinetics of adsorbtion on carbon from solution, Journal of Sanitay Engineering Division, American Society of Civil Engineers 89 (1963) 31.
[36] Y.S. Ho, G.A. McKay, Comparison of chemisorption kinetic models applied to pollutant removal on various sorbents, Transaction of the International Chemical Engineering 76B (1998) 332–340.
[37] I.L. Jenkins, A.G. Wain, Extraction of molybdenum from radioactive wastes, Journal of Applied Chemistry of the USSR 14/10 (1964) 449.
[38] O.N. Kononova, A.G. Kholmogorov, S.V. Kachin, O.P. Kalyakina, E.V. Sadovskaya, Ion exchange recovery of molybdenum from nitric acid solution using macroporous anion exchanger with long-chained cross-linking agents, Hydrometallurgy 68 (2003) 83–87.
[39] S.M. Le, A.P. Davis, Removal of Cu(II) and Cd(II) from aqueous solution by seafood processing waste sludge, Water Research 35 (2001) 534–540.